Title

Activation of Cytosolic Cathepsin B Activity in the Brain by Traumatic Brain Injury and Inhibition by the Neutral pH Selective Inhibitor Probe Z-Arg-Lys-AOMK.

Authors

Podvin, Sonia

Florio, Jazmin

Spencer, Brian

et al.

Publication Date

2025-03-25

DOI

10.1021/acschemneuro.4c00577

Peer reviewed

ACS Chemical Neuroscience

pubs.acs.org/chemneuro
Research Article

Activation of Cytosolic Cathepsin B Activity in the Brain by Traumatic Brain Injury and Inhibition by the Neutral pH Selective Inhibitor Probe Z-Arg-Lys-AOMK

Sonia Podvin, Jazmin Florio, Brian Spencer, Michael Mante, Estefani Guzman, Carlos Arias, Charles Mosier, Von V. Phan, Michael C. Yoon, Jehad Almaliti, Anthony J. O'Donoghue, William H. Gerwick, Robert A. Rissman, and Vivian Hook*

Cite This: ACS Chem. Neurosci. 2025, 16, 1297−1308
Read Online

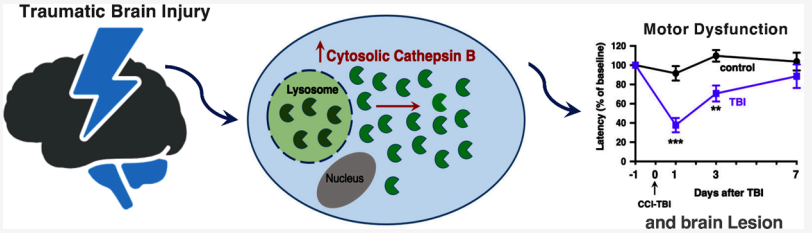

ABSTRACT: Cathepsin B has been shown to contribute to deficits in traumatic brain injury (TBI), an important risk factor for Alzheimer's disease (AD). Cathepsin B is elevated in TBI and AD patients, as well as in animal models of these conditions. Knockout of the cathepsin B gene results in amelioration of TBI-induced motor dysfunction and improvement of AD memory deficit in mice. The mechanism of cathepsin B pathogenesis in these brain disorders has been hypothesized to involve its translocation to the cytosol from its normal lysosomal location. This study, therefore, evaluated brain cytosolic cathepsin B activity in the controlled cortical impact (CCI) mouse model of TBI. CCI-TBI resulted in motor deficits demonstrated by the rotarod assay, brain tissue lesions, and disorganization of the hippocampus. Significantly, CCI-TBI increased cytosolic cathepsin B activity in the brain cortex in the ipsilateral brain hemisphere that received the CCI-TBI injury, with a concomitant decrease in the lysosomal fraction. Cathepsin B activity was monitored using the substrate Z-Nle-Lys-Arg-AMC which specifically detects cathepsin B activity but not other cysteine proteases. The normal lysosomal distribution of cathepsin B was observed by its discrete localization in brain cortical cells. CCI-TBI resulted in a more diffuse cellular distribution of cathepsin B consistent with translocation to the cytosol. Further studies utilized the novel neutral pH-selective inhibitor, Z-Arg-Lys-AOMK, that specifically inhibits cathepsin B at neutral pH 7.2 of the cytosol but not at acidic pH 4.6 of lysosomes. Daily administration of Z-Arg-Lys-AOMK (ip), beginning 1 day before CCI-TBI, resulted in the reduction of the increased cytosolic cathepsin B activity induced by CCI-TBI. The inhibitor also reduced cathepsin B activities in homogenates of the brain cortex and hippocampus which were increased by CCI-TBI. Furthermore, the Z-Arg-Lys-AOMK inhibitor resulted in the reduction of motor function deficit resulting from CCI-TBI. These findings demonstrate the activation of cytosolic cathepsin B activity in CCI-TBI mouse brain injury.

KEYWORDS: *traumatic brain injury, cathepsin B, cytosol, motor dysfunction, brain lesion, inhibitor*

INTRODUCTION

The cysteine protease cathepsin B has been shown to participate in behavioral deficits of traumatic brain injury (TBI), an important risk factor for the development of Alzheimer's disease (AD) and related brain disorders.[1] In TBI patients, cathepsin B is elevated and correlates with the severity of injury.[2,3] In AD patients, increased cathepsin B correlates with cognitive deficits.[4,5] Mouse models of TBI and AD display elevated cathepsin B in the brain.[1] Cathepsin B gene knockout in these models results in the amelioration of motor deficits in TBI[6] and reduces memory loss and decreases amyloid-β (Aβ) in AD mice.[7,8] Also, in a periodontitis AD mouse model, knockout of cathepsin B ameliorates memory deficit.[9] Moreover, TBI is a risk factor for the development of not only AD but also related brain disorders including dementia and stroke.[10−12] These findings demonstrate the participation of cathepsin B in the behavioral deficits associated with TBI and AD.

Received: September 4, 2024
Revised: January 30, 2025
Accepted: March 11, 2025
Published: March 25, 2025

https://doi.org/10.1021/acschemneuro.4c00577
ACS Chem. Neurosci. 2025, 16, 1297−1308

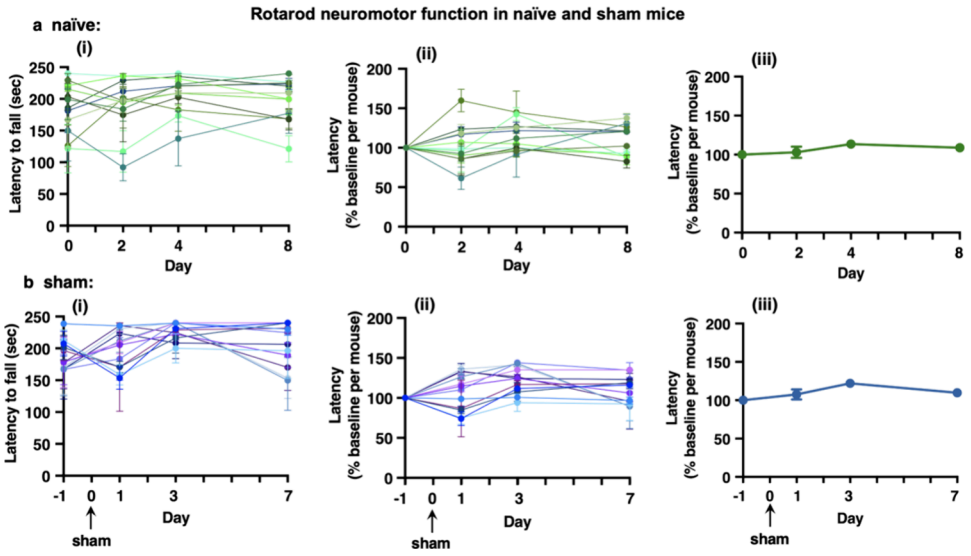

Figure 1. Rotarod neuromotor function in naïve and sham mice. (a) Naïve mice. Naïve mice were evaluated for motor function by rotarod assays over several days numbered as 0, 2, 4, and 8 days. The data for latency time to fall for each mouse (12 adult mice, females) were plotted, showing the mean ± sem of three trials conducted on the designated day (panel i). The rotarod latency was also plotted as % baseline latency relative to day 0 for individual mice (panel ii). The mean ± sem latency rotarod data (% baseline latency) (panel iii) was plotted and showed reproducibility in rotarod data from day to day. (b) Sham mice. Mice were subjected to a sham procedure consisting of anesthesia and incision of the skin above the head to expose the skull, conducted on day "0". Rotarod performance assays were conducted on days 1, 3, and 7 after the sham procedure, and compared to baseline rotarod latency conducted 1 day before the sham procedure. Rotarod latency data (secs) were plotted for the individual mice (12 adult mice total, female) (panel i) and also plotted as % baseline latency for individual mice (panel ii). The mean ± sem data for % baseline latency was plotted for the group of 12 mice (panel iii).

The mechanism of cathepsin B in deficits of TBI and AD, as well as in related brain disorders, has been hypothesized to involve lysosomal leakage and translocation of the normal lysosomal cathepsin B to the pathogenic, cytosolic location of cathepsin B[1] where the enzyme induces cell death[13,14] and inflammation.[15−17] TBI induction of cytosolic cathepsin B has been observed by cellular brain imaging in a central fluid percussion model of TBI.[18] In an APOE4 mouse model of AD, pathogenesis resulted in lysosomal leakage observed by imaging of a lysosomal marker (cathepsin D) which occurred with cognitive deficits and increased Aβ.[19] In neuronal cells, pathogenic Aβ-induced lysosomal leakage was observed by imaging with lucifer yellow or acridine orange.[20,21] Mechanical shearing of neurons in culture resulted in lysosomal membrane permeability damage.[22] While these data suggest the translocation of cathepsin B to the cytosol, direct evaluation of increased cytosolic cathepsin B activity in TBI or AD conditions has not yet been demonstrated.

Therefore, this study investigated cytosolic cathepsin B activity in the brains of the controlled cortical impact (CCI) mouse model of TBI. Notably, CCI-TBI resulted in the elevation of cytosolic cathepsin B activity in the cerebral cortex of the brain (referred to as cortex in this study). CCI-TBI induction of cathepsin B activity was also observed in tissue homogenates from the cortex and hippocampus brain regions. CCI-TBI increased the diffuse cytosolic distribution of cathepsin B and reduced the normal punctate, discrete localization of cellular lysosomal cathepsin B in the brain. Moreover, administration of the neutral pH selective inhibitor Z-Arg-Lys-AOMK, a specific inhibitor of cathepsin B,[23] to CCI-TBI mice resulted in substantial inhibition of cytosolic cathepsin B activity in the brain. Further, the inhibitor reduced CCI-induced motor dysfunction. These results were conducted in female mice because more severe TBI outcomes have been observed in females compared to males[24−28] which include depression and anxiety combined with higher mortality risk. Overall, the results demonstrate that CCI-TBI activates cytosolic cathepsin B proteolytic activity that may participate in TBI deficits.

RESULTS

Analysis of Motor Function by Rotarod Performance: Variance, Sham Control Conditions, and Controlled Cortical Impact (CCI) TBI. *Rotarod Latencies of Motor Function among Individual Naïve Mice.* In this study, we first characterized quantitative rotarod performance assays of motor function in normal mice to assess variance. Rotarod data were assessed among individual naïve wild-type adult mice (adult, 4−5 months of age, female) before beginning CCI-TBI experiments. The rotarod assay measures the latency time during which each animal maintains their presence on a rotating rod.[6] We analyzed the range of baseline latencies in naïve mice on several days during a period of 1 week (Figure 1a). The data show a range of rotarod latencies from 80 to 240 s (Figure 1a,i). The experimental goal is to evaluate each individual mouse for differences in baseline latency compared to that after CCI-TBI. Therefore, latency data were analyzed as the percent of normal latency for each animal, as shown for naïve mice on days 0, 2, 4, and 8 (Figure 1a,ii). The mean rotarod performance for the group of naive animals assessed as a percent of baseline latency shows consistency over several days during a period of about 1 week (Figure 1a,iii).

Comparison of Rotarod Performance in Sham Mice Compared to Naïve Mice. Rotarod performance was assessed after a sham procedure during which mice were under anesthesia and had an incision of the skin at the top of the head scalp, which exposed the skull cap. The motor function of these sham mice was assessed 1 day before the sham procedure

https://doi.org/10.1021/acschemneuro.4c00577
ACS Chem. Neurosci. 2025, 16, 1297−1308

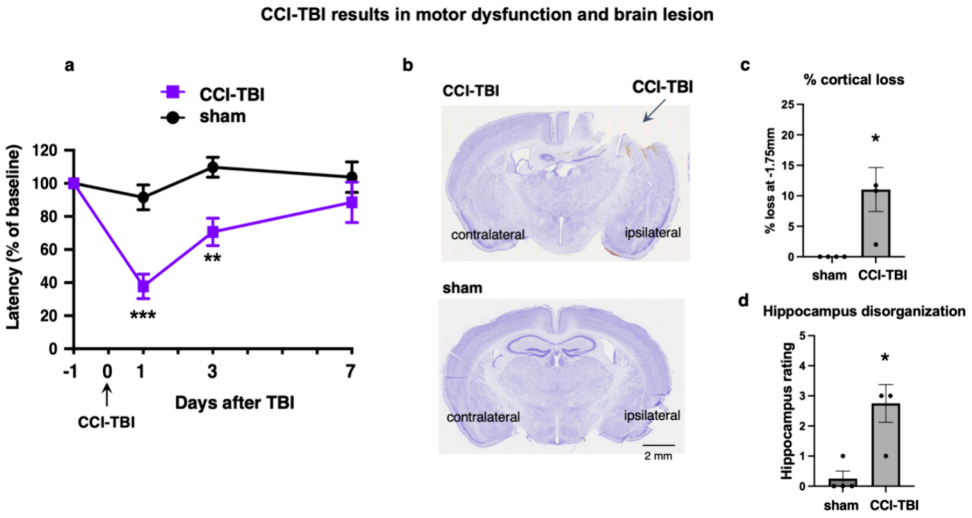

Figure 2. CCI-TBI results in motor dysfunction and brain lesion. (a) Motor function deficit in CCI-TBI mice. Mice were subjected to CCI-TBI or sham procedures, and rotarod motor function was assessed on days 1, 3, and 7 after CCI-TBI or sham. Latencies for rotarod data are expressed as % of baseline latency, shown as mean ± sem for CCI-TBI (n = 9) and sham (n = 7). Statistical significance of CCI-TBI compared to sham was assessed by student's t test (**p < 0.01, ***p < 0.001) for comparison of CCI-TBI with sham control at each time point. In addition, ANOVA analysis of the CCI-TBI animals for comparison of rotarod data at baseline and on days 1, 3, and 7 after CCI-TBI found significant difference between day 1 and baseline rotarod performance measurements. (b) Brain cortical lesion after by CCI-TBI. Brain sections were analyzed for cortical brain lesions by Nissl staining in CCI-TBI and sham mice, post-TBI on day 2. The ipsilateral hemisphere of the brain cortex received the CCI injury, and the contralateral hemisphere was not subjected to injury. (c) Quantitation of cortical tissue lesions. Quantitation of brain cortical tissue lesions on day 2 after CCI-TBI was conducted by image analysis. Data are illustrated as mean ± sem; significance was assessed by student's t test (*p < 0.05). (d) Hippocampal disorganization. Disorganization of the hippocampus structural integrity on day 2 after CCI-TBI was evaluated by Nissl staining and assessed a rating scale of 0−4 for relative levels of tissue integrity, cell loss, and disorganization, as shown in supplemental Figure S2. The rating for integrity to disorganized hippocampus is evaluated as mean ± sem with significance assessed by student's t test (p < 0.05).

and on days 1, 3, and 7 after the sham procedure. The rotarod data were analyzed as latency times (secs) and as % of baseline latency for each animal (Figure 1b, parts i,ii). The latency time data show a range of baseline rotarod latencies. The percent of baseline latencies shows the ranges of latencies compared with the baseline for each animal. The consistency of the mean percent of baseline rotarod latencies at several time points after the sham procedure (Figure 1b, part iii) appears similar to that of the naïve mice (Figure 1a, part iii). Since this sham condition did not affect normal motor function, this sham condition was used in this CCI-TBI study.

We also assessed a modified sham condition that consisted of a craniotomy that removed a skull cap area of 5 mm circumference, conducted after a skin incision at the scalp. Rotarod analysis 1 day before this modified sham condition and on subsequent days was assessed. Results showed that the rotarod latency was significantly decreased 1 day after the modified sham procedure, and the latency recovered to baseline levels at 3 and 7 days (supplementary Figure S1). These data show that the craniotomy procedure resulted in the diminution of motor function and, thus, did not represent a control for CCI-TBI experiments. These data show that the craniotomy step used in the TBI procedure contributes to the diminution of motor dysfunction.

For the CCI-TBI experiments of this study, it was important to demonstrate a sham control condition that does not alter the rotarod motor performance. A comparison of the two conditions of scalp incision versus craniotomy (with scalp incision) found that only the scalp incision alone had no effect on the rotarod performance. Therefore, the scalp incision sham condition was used as a control for this CCI-TBI study.

CCI-TBI Motor Deficits. CCI brain injury was directed to the right brain cortex as described in the methods, located at 0.5−5.5 mm posterior of bregma and 1−6 mm right of the sagittal suture. CCI was conducted using a 3 mm impactor tip at a speed of 3 m/s to a depth of 1 mm with a 100 ms dwell time. Neuromotor function was assessed by the rotarod assay on days 1, 3, and 7 after CCI and compared to baseline motor function conducted 1 day prior to CCI, as well as to sham controls. CCI resulted in substantial motor deficits on days 1 and 3 after CCI which showed latency times of about 40% and 70% of baseline function prior to CCI (Figure 2a). Sham control mice showed consistent normal motor function during the time course of 1−7 days.

CCI injury was confirmed by a brain morphological lesion at the site of CCI of the brain cortex, as illustrated by histological Nissl staining on day 2 after CCI (Figure 2b). Sham mice displayed intact cortical tissue, with no lesions. Quantitative imaging for the percent loss of cortical tissue showed that CCI-TBI resulted in the loss of brain cortical tissue compared to sham (Figure 2c). Furthermore, CCI-TBI also caused disorganization of the hippocampal brain tissue (Figure 2d), assessed by a rating scale for integrity and disorganization of hippocampus morphology, including cell loss. The rating scale for modest to severe hippocampal structural disorganization is illustrated in supplemental Figure S2.

Increase in Cytosolic Cathepsin B Activity after CCI-TBI. *CCI-TBI Increases Cathepsin B Activity in the Cortex and Hippocampus.* CCI-TBI induced activation of cathepsin B proteolytic activity in brain homogenates from the cortex and hippocampus regions when compared to sham controls (Figure 3). Significant increases in cathepsin B activity were observed for these regions in the ipsilateral hemisphere of the

https://doi.org/10.1021/acschemneuro.4c00577
ACS Chem. Neurosci. 2025, 16, 1297−1308

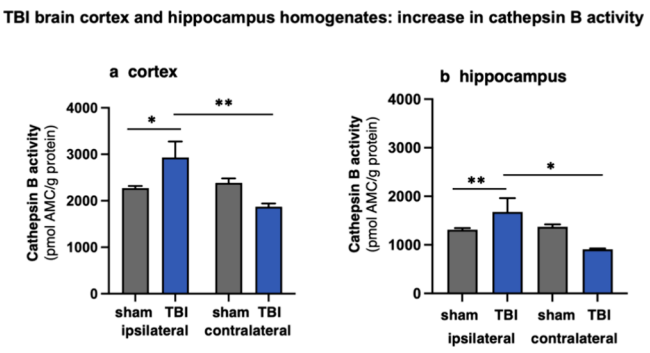

Figure 3. TBI brain cortex and hippocampus tissue homogenates: increase in cathepsin B activity. (a) Brain cortex. Cathepsin B activities were measured in homogenates of brain cortex from CCI-TBI and sham control mice on day 8 after CCI-TBI. Ipsilateral and contralateral hemispheres of each brain region were assayed separately. Cathepsin B activity in homogenate was measured at pH 5.5, representing an intermediate pH between cytosolic pH 7.2 and lysosomal pH 4.6. Data are displayed as cathepsin B activity (pmol AMC/μg protein per 30 mn. assay), mean ± sem (CCI-TBI, n = 5; sham, n = 7) analyzed by student's t test (*p < 0.05, **p < 0.01, ***p < 0.001). (b) Brain hippocampus. Cathepsin B activities in hippocampus homogenates, from ipsilateral and contralateral hemispheres, were measured as described for brain cortex (panel a), assessed on day 8 after CCI-TBI. Cathepsin B was assayed at pH 5.5. Data for CCI-TBI and sham mice (CCI-TBI, n = 4; sham, n = 7) were analyzed by student's t test (*p < 0.05, ***p < 0.001).

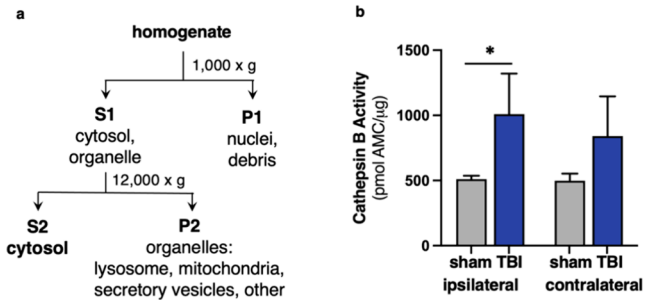

Figure 4. Increase in cytosolic cathepsin B activity in brain cortex induced by CCI-TBI. (a) Cytosol isolation by fractionation of brain cortex. After CCI-TBI and sham procedures combined with rotarod testing, brains were collected on day 8 after CCI-TBI, and the cytosol fraction was isolated from brain cortex homogenates by differential centrifugation to obtain the S2 cytosol fraction, separated from organelles of lysosomes, mitochondria, secretory vesicles, nuclei, and other organelles.[28,29] (b) Increased cathepsin B activity in cytosol of the brain cortex after CCI-TBI. Cathepsin B activity analysis was conducted on day 8 after CCI-TBI. Cathepsin B activity in cytosol of the brain cortex (ipsilateral and contralateral) was assayed at pH 5.5 (as pmol AMC/μg protein per 30 min assay). Assay at pH 5.5 was selected to assess cathepsin B activity in the cytosol under the same pH condition as the assay of the cortex homogenate conducted at pH 5.5 (Figure 3), which is an intermediate pH between lysosomal pH 4.6 and cytosolic pH 7.2. Data are evaluated as mean ± sem for CCI-TBI and sham mice (CCI-TBI, n = 5; sham, n = 7) analyzed by student's t test (*p < 0.05, **p < 0.01, ***p < 0.001). When the cortex cytosol was assayed at the cytosolic pH of 7.2,[44] results also showed higher cathepsin B activity in the ipsilateral cortex compared to the contralateral cortex from CCI-TBI mice. Thus, assay at both pH 5.5 and pH 7.2 showed increased cathepsin B activity in the cytosol of brain cortex from CCI-TBI mice.

brain that received the CCI-TBI injury but not observed on the contralateral side that had no injury. It is noted that higher cathepsin B specific activity was observed in the cortex compared to that in the hippocampus brain tissues (Figure 3).

Cathepsin B activity was measured using our recently developed fluorogenic substrate Z-Nle-Lys-Arg-AMC, which is specifically cleaved by cathepsin B and is not cleaved by other cysteine cathepsin proteases.[29] Therefore, the Z-Nle-Lys-Arg-AMC cleaving activity specifically represents the cathepsin B activity.

Cytosolic Cathepsin B Activity Is Increased by CCI-TBI. To assess the hypothesis that CCI-TBI results in the elevation of cytosolic cathepsin B, subcellular fractionation of the brain cortex was conducted to isolate the cytosol fraction (Figure 4a). CCI-TBI resulted in increased cytosolic cathepsin B activity in the brain cortex when compared to sham control, monitored by the specific substrate Z-Nle-Lys-Arg-AMC (Figure 4b). A significant increase in cathepsin B activity was observed in the cytosol from the ipsilateral hemisphere of the brain cortex after CCI-TBI, which displayed increased cathepsin B activity by about 2-fold over sham control. The contralateral cortex cytosol showed an increase in cathepsin B activity of ∼ 50% compared to sham but did not reach statistical significance. These data indicate increased cathepsin B activity in the cytosol of the ipsilateral brain cortex that was induced by CCI-TBI.

The increase in cytosolic cathepsin B during CCI-TBI has been hypothesized to result from lysosomal leakage and translocation of lysosomal cathepsin B to the cytosol.[1] This hypothesis predicts that lysosomal cathepsin B may be decreased during CCI-TBI. Evaluation of the lysosomal fraction (P2 fraction, prepared as shown in Figure 4a), showed decreased levels of lysosomal cathepsin B activity, occurring with increased levels of cytosolic cathepsin B activity (supplemental Figure S3). These data are consistent with the hypothesis of the translocation of lysosomal cathepsin B to the cytosol during CCI-TBI.

Translocation of Cathepsin B to the Cytosol Indicated by Decreased Punctate Lysosomal Localization and Increased Diffuse Cytosolic Localization in CCI-TBI Mouse Brain Cells. Brain sections were analyzed for the normal, discrete pattern of lysosomal cathepsin B localization in control sham mice and compared to CCI-TBI induction of the more diffuse cytosolic distribution of cathepsin B in brain cortical cells (Figure 5). The percent of cathepsin B observed as discrete, punctate lysosomal localization was assessed by quantitative immunofluorescence imaging. Results showed that CCI-TBI resulted in decreased punctate, lysosomal cathepsin B localization compared to the sham control (Figure 5a,b). Notably, CCI-TBI increased the diffuse presence of cathepsin B enzyme in cells, consistent with its cytosol-like distribution, observed 2 days after CCI-TBI (Figure 5a). These results were observed in the ipsilateral cortex that was subjected to impact injury. The increase in cytosolic cathepsin B continued to day 8 after CCI-TBI (Figures 5b and S4). These data suggest that CCI-TBI increased the diffuse localization of cytosolic cathepsin B, differing from the normal lysosomal cathepsin B, which is consistent with elevated cathepsin B activity in the cytosol (Figure 4).

Neutral pH-Selective Inhibitor Z-Arg-Lys-AOMK of Mouse Cathepsin B Reduces Increased Cytosolic Cathepsin B in the CCI-TBI Brain. *Mouse Cathepsin B Is*

https://doi.org/10.1021/acschemneuro.4c00577
ACS Chem. Neurosci. 2025, 16, 1297−1308

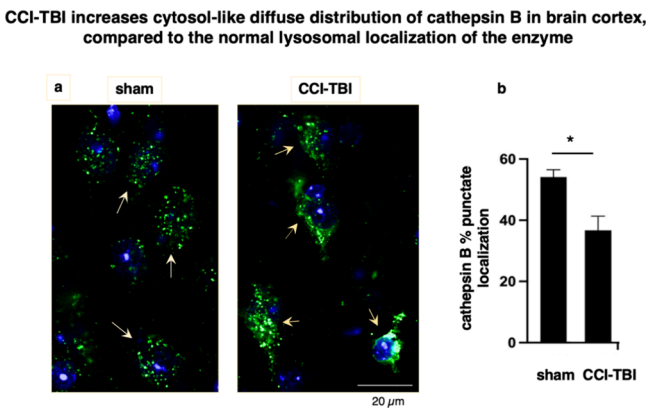

Figure 5. CCI-TBI increased cytosol-like diffuse distribution of cathepsin B in brain cortex, compared to the enzyme's normal lysosomal localization. (a) Immunofluorescence imaging illustrates reduction in cathepsin B lysosomal localization and increased cytosol-like distribution in brain after CCI-TBI. Brain cortex sections from CCI-TBI and sham mice were analyzed for cathepsin B cellular distribution by immunofluorescence (green) imaging microscopy, on day 2 after CCI-TBI or sham. The control sham condition showed normal discrete, punctate localization of lysosomal cathepsin B that was located near nuclei (stained with DAPI blue). However, in the CCI-TBI condition, cathepsin B showed a more diffuse cytosol-like distribution throughout cells and diminished punctate lysosomal localization. (b) Quantitation of reduced punctate lysosomal cathepsin B localization after CCI-TBI. Quantitation of immunofluorescence anticathepsin B images showed a significant decrease punctate localization in CCI-TBI compared to sham control, observed on day 8 after CCI-TBI (*$p < 0.05$, by student's t test).

Selectively Inhibited by Z-Arg-Lys-AOMK at Cytosolic Neutral pH 7.2, Rather Than at the Acidic Lysosomal pH of 4.6. We recently developed the neutral pH-selective inhibitor, Z-Arg-Lys-AOMK, of cathepsin B, which displays nanomolar potency to inhibit human cathepsin B at the neutral pH 7.2 of the cytosol.[23] This novel inhibitor was found to be 100 times more effective to inhibit human cathepsin B at a neutral pH of 7.2 compared to the acidic pH of 4.6 of the lysosome. Also, Z-Arg-Lys-AOMK specifically inhibits human cathepsin B without inhibition of other cysteine cathepsins.[26]

Importantly, for this mouse CCI-TBI study, it was important to assess this inhibitor for potent inhibition of mouse cathepsin B. We, therefore, assessed the ability of this inhibitor to reduce mouse cathepsin B activity with respect to potency and pH selectivity (Figure 6). Mouse cathepsin B activity was potently reduced by Z-Arg-Lys-AOMK at neutral pH 7.2 with a low IC_{50} value of 25 nM (IC_{50}, inhibitor concentration for the reduction of activity by 50%). However, poor inhibition occurred at acidic pH 4.6, with a high IC_{50} value of 2500 nM. These data show that mouse cathepsin B, like human cathepsin B, is potently inhibited by Z-Arg-Lys-AOMK at nM levels at neutral pH which is 100 times more effective than its poor inhibition at acidic pH 4.6.

With respect to specificity for mouse cathepsin B over other cysteine cathepsins at neutral pH 7.2, Z-Arg-Lys-AOMK was found to specifically inhibit mouse cathepsin B compared with other mouse cathepsins C, H, L, and X (supplemental Table S1). Mouse cathepsins C, H, and L were not affected by Z-Arg-Lys-AOMK at 10 and 100 nM. At a higher concentration of 1 μM Z-Arg-Lys-AOMK, cathepsins C and H were not affected, and mouse cathepsin C activity was decreased by 28%

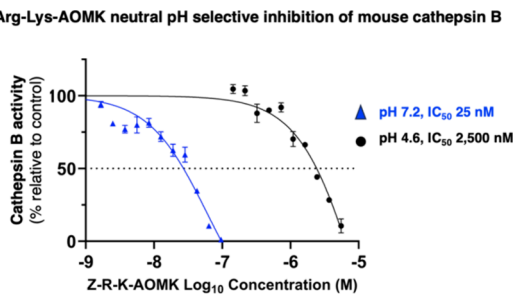

Figure 6. Z-Arg-Lys-AOMK neutral pH selective inhibition of mouse cathepsin B. The effectiveness of Z-Arg-Lys-AOMK to inhibit purified, recombinant mouse cathepsin B was assessed at the cytosolic neutral pH of 7.2[44] and compared to the lysosomal acidic pH 4.6,[45] at nM to μM concentrations of inhibitor. The concentration to inhibit cathepsin B by 50% at each pH was determined as IC_{50} values of 25 nM at pH 7.2 and 2500 nM at pH 4.6. These data indicate highly effective Z-Arg-Lys-AOMK inhibition of cathepsin B at neutral pH 7.2, and 100-fold less inhibitory effectiveness at acidic pH 4.6.

(supplemental Table S1). Mouse cathepsin X showed no activity at pH 7.2. At acidic pH 4.6, Z-Arg-Lys-AOMK at 0.1 μM, 1 μM, and 10 μM had no effect on mouse cathepsins C, H, L, and X activities (supplemental Table S2). These results demonstrate the selectivity of Z-Arg-Lys-AOMK to potently inhibit mouse cathepsin B (Figure 6), without inhibiting other mouse cysteine cathepsins C, H, and L at comparable concentrations (supplemental Table S1).

It was of interest to find that the specific activity of mouse cathepsin B was greater at pH 7.2 than at pH 4.6 (supplemental Table S3). This property of high specific cathepsin B activity at neutral pH 7.2 supports the observation of elevated cathepsin B activity in the CCI-TBI brain (Figures 3 and 4) after its translocation from cellular lysosomes to the cytosol (Figure 5).

CCI-TBI Activation of Cytosolic Cathepsin B Activity in the Brain Is Reduced by the Administration of the Neutral pH-Selective Inhibitor Z-Arg-Lys-AOMK. The Z-Arg-Lys-AOMK inhibitor was administered by ip (intraperitoneal injection) at 20 mg/kg daily, beginning 1 day prior to CCI-TBI. Vehicle buffer was administered as a control to CCI-TBI mice. Brain cortex and hippocampus tissues were collected and evaluated for cathepsin B activity on the sixth day after CCI-TBI. In the cytosol of CCI-TBI mouse brain cortex (ipsilateral), Z-Arg-Lys-AOMK treatment resulted in reduced cathepsin B activity (Figure 7a) that was increased by CCI-TBI (Figure 4). The inhibitor also reduced cathepsin B activity in brain homogenate (ipsilateral) of CCI-TBI mice (Figure 7b,c), showing that the inhibitor reduced the CCI-TBI-induced increase in cathepsin B activity in the brain cortex and hippocampus.

It was of interest to note that Z-Arg-Lys-AOMK had no effect on lysosomal cathepsin B activity in the contralateral cortex, but this inhibitor reduced cathepsin B in the ipsilateral cortex lysosomal fraction during CCI-TBI (Supporting Information, Figure S6). These data demonstrate differences in Z-Arg-Lys-AOMK sensitivity of contralateral versus ipsilateral cortical cathepsin B in the lysosomal fraction during CCI-TBI.

Significantly, the Z-Arg-Lys-AOMK inhibitor improved motor deficit in CCI-TBI mice, indicated by rotarod motor function assays conducted 1 day after brain injury (Figure 8a). The CCI-TBI motor deficit was observed as about 35% rotarod latency compared to the normal 100% baseline latency

https://doi.org/10.1021/acschemneuro.4c00577
ACS Chem. Neurosci. 2025, 16, 1297−1308

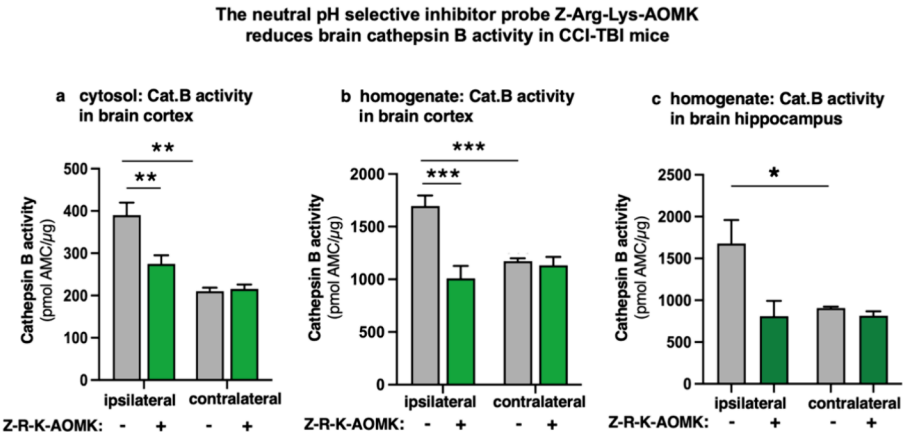

Figure 7. The neutral pH selective inhibitor probe Z-Arg-Lys-AOMK reduces cytosolic cathepsin B activity in CCI-TBI brain. (a) Z-Arg-Lys-AOMK reduced cytosolic cathepsin B activity in brain cortex of CCI-TBI mice. The neutral pH selective inhibitor probe Z-Arg-Lys-AOMK of cathepsin B was administered (20 mg/kg/day, ip) to mice beginning 1 day before CCI-TBI, and continued with daily administration through day 6 after CCI-TBI. The 6 day time point after TBI was selected as a time when recovery from motor deficits occurred (at 6−7 days), compared to significant motor deficits at 1−3 days after CCI-TBI (Figure 2a). Inhibitor administration was conducted each day at 10−11 am in the morning. Mice were sacrificed on day 6 and the cytosol fraction was isolated from brain cortex. Cathepsin B activity (measured at pH 7.2) in the cytosol was assayed and evaluated as pmol AMC/μg protein in 30 min assays under the conditions of CCI-TBI and inhibitor (n = 4) and CCI-TBI with vehicle control (n = 6). Data are displayed as the mean ± sem and assessed for significance by student's t test (**p < 0.01). (b) Z-Arg-Lys-AOMK reduced cathepsin B activity in brain cortex homogenate from CCI-TBI mice. TBI-CCI mice were treated with the Z-Arg-Lys-AOMK inhibitor as described in panel "a" of this figure, and brain tissue was collected on day 6 after CCI-TBI. Cathepsin B activity in brain cortex homogenate (measured at pH 7.2) was assayed and displayed as the mean ± sem of pmol AMC/μg protein (30 min cathepsin B assay) for the conditions of CCI-TBI and inhibitor (n = 4) and CCI-TBI with vehicle control (n = 6). Student's t test was utilized to assess significance (***p < 0.001). (c) Z-Arg-Lys-AOMK reduced cathepsin B activity in brain hippocampus homogenate from CCI-TBI mice. CCI-TBI mice were treated with the inhibitor as described in panel 'a' of this figure, and hippocampus was collected on day 6 after CCI-TBI. Cathepsin B activity was assayed (pH 7.2) and the calculated as the mean ± sem of pmol AMC/μg protein (30 min assay) for CCI-TBI treated with inhibitor (n = 4) and CCI-TBI treated with vehicle control (n = 6). Comparisons were assessed by student's t test (***p < 0.001).

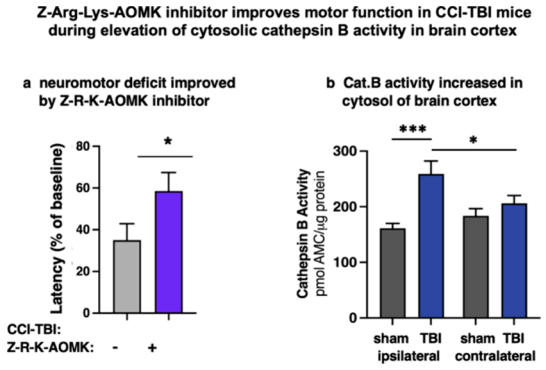

Figure 8. Z-Arg-Lys-AOMK inhibitor improves motor function in CCI-TBI mice during elevation cytosolic cathepsin B activity in brain cortex. (a) Rotarod motor deficit was improved by Z-Arg-Lys-AOMK. CCI-TBI mice were administered Z-Arg-Lys-AOMK (n = 4) or vehicle control (n = 6) daily beginning 1 day before CCI-TBI. Z-Arg-Lys-AOMK administration occurred at 10−11 am in the mornings. Mice were assessed for rotarod motor performance on day 1 after CCI-TBI. The rotarod latency, expressed as % of baseline, is illustrated as the mean ± sem, with significance assessed by student's t test (*p < 0.05). (b) Increased cathepsin B activity in cytosol of brain cortex during CCI-TBI motor deficit. Cathepsin B activity was measured at pH 7.2 for the cytosol fraction isolated from brain cortex, collected on day 2 after CCI-TBI. Cytosol isolation was conducted for ipsilateral and contralateral brain cortex. Cathepsin B activity in CCI-TBI and sham mice (n = 10 per group) was assessed as the mean ± sem, with significance between conditions assessed by student's t test (*p < 0.05, ***p < 0.001).

at 1 day prior to CCI-TBI. Treatment of CCI-TBI mice resulted in a longer latency time in the rotarod assay, of about 55% latency compared to 100% normal baseline control. The motor deficit was associated with increased cathepsin B activity observed on day two after CCI-TBI (Figure 8b).

These findings demonstrate that Z-Arg-Lys-AOMK can inhibit cytosolic cathepsin B in the brain cortex of CCI-TBI mice and can improve motor deficits achieved by peripheral ip administration.

DISCUSSION

Results demonstrated that CCI-TBI resulted in a significant elevation of cytosolic cathepsin B activity in the brain cortex region of female mice. Increases in cytosolic cathepsin B activity occurred primarily in the ipsilateral, as well as contralateral, cortex after CCI-TBI. Cathepsin B activities in tissue homogenates of the cortex and hippocampus were also increased after CCI-TBI. CCI-TBI increased the diffuse localization of cytosolic cathepsin B, combined with a decrease in its punctate localization to lysosomes, demonstrated by immunofluorescence imaging of cathepsin B. The increased cytosolic cathepsin B activity in the brain was blocked by Z-Arg-Lys-AOMK, a novel neutral pH selective inhibitor probe of cathepsin B that we recently developed.[23] This inhibitor was administered by intraperitoneal (ip) injection (20 mg/kg/day) and resulted in decreased cathepsin B activity in the cytosol of the brain cortex and in homogenates of the cortex and hippocampus. These data show that the inhibitor can cross the blood-brain barrier to inhibit the cathepsin B target in the brain. Furthermore, Z-Arg-Lys-AOMK inhibitor treatment of CCI-TBI mice resulted in improved motor deficit at 1 day after

https://doi.org/10.1021/acschemneuro.4c00577
ACS Chem. Neurosci. 2025, 16, 1297−1308

CCI-TBI. These findings demonstrate that CCI-TBI brain injury activates cathepsin B activity in the cytosol, which is associated with behavioral deficits in motor function.

It was important for this study to determine a sham condition that maintained normal motor function, as assessed by rotarod assays. We compared rotarod performance in naïve mice and two "sham" conditions of mice subjected to skin incision at the scalp and mice subjected to craniotomy removal of the skull cap (5 mm section) after scalp skin incision. Scalp incision alone had no effect on the normal rotarod performance displayed by naïve mice. However, craniotomy resulted in diminished rotarod performance at 1 day after skull cap removal. These data show that the scalp skin incision procedure does not affect the rotarod function. However, craniotomy with skull cap removal after scalp incision was detrimental to the rotarod performance. Therefore, the scalp skin incision procedure was used as a sham condition with no effect on rotarod performance, since it was important for the sham control to represent normal naive mice.

This study utilized our newly developed Z-Nle-Lys-Arg-AMC fluorogenic substrate that specifically monitors cathepsin B activity and not other cysteine cathepsin proteases.[29] The advantage of Z-Nle-Lys-Arg-AMC over other substrates used to measure cathepsin B activity, Z-Phe-Arg-AMC, and Z-Arg-Arg-AMC, is its specificity for cathepsin B compared to other cysteine cathepsins and greater sensitivity for monitoring cathepsin B activity over a broad pH range.[29] Importantly, Z-Nle-Lys-Arg-AMC is cleaved by cathepsin B at neutral pH and thus allows the assay of cathepsin B in the brain cytosol fraction at neutral pH. The sensitive and specific Z-Nle-Lys-Arg-AMC substrate allowed analysis of cytosolic cathepsin B activity at neutral pH in the brains of CCI-TBI mice in this study.

The increased cytosolic cathepsin B activity in the brains of mice subjected to CCI-TBI was inhibited by treatment of mice (ip administration) with the novel neutral pH selective inhibitor of cathepsin B, Z-Arg-Lys-AOMK. This inhibitor was developed by modifying the neutral pH-selective substrate Z-Arg-Lys-AMC with the C-terminal acyloxymethyl ketone (AOMK) warhead to generate the potent and specific Z-Arg-Lys-AOMK inhibitor.[23] This inhibitor potently inhibits mouse and human cathepsin B at nM levels, with 100-fold selectivity for inhibition at neutral cytosolic pH 7.2 compared to acidic lysosomal pH 4.6. Results showed that Z-Arg-Lys-AOMK inhibited cytosolic cathepsin B activity *in vivo* in the CCI-TBI mouse brain, indicating that the inhibitor penetrates the blood-brain barrier to reach the brain. Notably, administration of Z-Arg-Lys-AOMK to CCI-TBI mice resulted in improved motor dysfunction at one-day after brain injury. These data suggest that the activated cytosolic cathepsin B may be involved in CCI-TBI injury.

The neutral pH selective inhibitor, Z-Arg-Lys-AOMK, may be predicted to target the neutral pH cytosolic cathepsin B associated with CCI-TBI, rather than the normal acidic lysosomal cathepsin B. Z-Arg-Lys-AOMK displays 100-fold more selectivity to inhibit neutral pH cathepsin B compared with the acidic cathepsin B activity. Thus, Z-Arg-Lys-AOMK may be predicted to display little effect on lysosomal cathepsin B. Indeed, this inhibitor had no effect on lysosomal fraction cathepsin B of the contralateral cortex of mice that received CCI-TBI in the ipsilateral cortex. However, Z-Arg-Lys-AOMK inhibited lysosomal cathepsin B of the ipsilateral cortex during CCI-TBI. These data suggest the hypothesis that in the ipsilateral cortex, lysosomal leakage could result in the equilibration of lysosomal pH to that of the cytosol, raising the lysosomal pH toward neutral pH, and allowing inhibition of lysosomal cathepsin B by Z-Arg-Lys-AOMK. But in the contralateral cortex, although lysosomal leakage occurs that reduces lysosomal cathepsin B, the lysosomes may be able to maintain their acidic pH, and, thus, the inhibition by Z-Arg-Lys-AOMK was not observed. This hypothesis will be worthy of investigation in future studies.

Importantly, CCI-TBI increased the diffuse cellular distribution of cathepsin B in the cytosol of the brain cortex, as observed by immunofluorescence microscopy, which contrasts with the normal punctate localization of cathepsin in lysosomes. These data are consistent with lysosomal leakage of cathepsin B into the cytosol during CCI-TBI. These findings support the hypothesis that the increase in cytosolic cathepsin B activity results from the translocation of lysosomal cathepsin B to the cytosol during CCI-TBI.

The importance of this study is that elevation of cytosolic cathepsin B activity in the CCI-TBI brain has been demonstrated, which has not been previously shown. Prior results in the field have reported that lysosomal cathepsin B becomes redistributed to the cytosol in disrupted brain neurons following central fluid percussion injury (CFPI) of the brain,[18] shown by immunofluorescence and electron microscopy of cathepsin B. In CFPI, treatment of animals with the cathepsin B inhibitor CA-074Me reduced hypersensitivity in the whisker nuisance behavioral task during elevated intracranial pressure,[30] indicating a role for cathepsin B in regulating somatosensory sensitivity in brain injury. Furthermore, increased intracranial pressure (ICP) (in rats) increased the diffuse localization of cathepsin B which is consistent with its redistribution to the cytosol from lysosomes.[31] Also, penetrating ballistic-like brain injury (PBBI) TBI in rats results in elevated cathepsin B in the brain cortex and hippocampus.[32] However, these TBI studies have not yet evaluated cathepsin B brain activity in the cytosol. This study provides new findings that cytosolic cathepsin B activity is elevated in CCI-TBI.

The novel results of this study showing elevated cytosolic cathepsin B activity and its inhibition by a neutral pH selective inhibitor in the CCI-TBI brain are relevant to other brain disorders that involve cathepsin B. Other TBI studies have reported increases in cathepsin B in the brains of animal models of CCI-TBI,[6,33] penetrating TBI conditions,[32] and diffuse TBI with intracranial pressure.[18,30,31] Elevation of cathepsin B has also been found in animal models and human patients of Alzheimer's disease, amyotrophic lateral sclerosis (ALS), stroke, aging, and related.[1] But studies of these brain disorders have not yet assessed cytosolic cathepsin B mechanisms. It will, therefore, be of interest to assess the roles of cytosolic pathogenic cathepsin B in TBI and related brain disorders.

Cytosolic cathepsin B in multiple cell types of neurons and microglia may contribute to cell death and inflammation that occur in TBI and related brain disorders. In neurons, cytosolic cathepsin B participates in cell death through proteolytic production of proapoptotic tBid, degradation of antiapoptotic Bcl-,[13,14] and induction of BAX, a pro-apoptotic cell death protein that is elevated during CCI-TBI.[6] In microglia, cytosolic cathepsin B activates the production of inflammatory IL-1β through the activation of the NLRP3 inflammasome.[34,35] For example, treatment of microglia (from mouse brain) with

https://doi.org/10.1021/acschemneuro.4c00577
ACS Chem. Neurosci. 2025, 16, 1297−1308

the neuropeptide chromogranin results in cathepsin B mediated production of IL-1β.[35] Analysis of cytosolic cathepsin B in neurons, microglia, and other cell types in the brain will be important to gain an understanding of the role of pathogenic, cytosolic cathepsin B in TBI and related brain disorders.

The role of cytosolic cathepsin B in cell death is consistent with findings from this study and others[6] that CCI-TBI results in loss of neurons, brain tissue lesions, and disorganization of hippocampus structural morphology. Future studies on the molecular pathways of cell death that are regulated by cytosolic cathepsin B will provide further insight into mechanisms of cytosolic cathepsin B regulation of cell death and neurodegeneration.

This study was conducted in female mice since more severe TBI deficits have been observed in females compared to males[24−28] involving TBI-related mental disturbances of depression and anxiety combined with high mortality risk.[24−26] It will be important for future studies to assess the role of cytosolic cathepsin B in males compared to females in TBI outcomes and deficits.

In summary, CCI-TBI results in significant activation of cytosolic cathepsin B activity in the brains of female mice, with the most pronounced increase occurring in the ipsilateral hemisphere of the brain cortex that received the CCI injury. The increased cytosolic cathepsin B activity in the mouse brain can be inhibited by the neutral pH-selective inhibitor of cathepsin B, Z-Arg-Lys-AOMK, that specifically targets cytosolic cathepsin B. Furthermore, the inhibitor reduced the severity of motor dysfunction resulting from CCI-TBI. These findings suggest a role for cytosolic cathepsin B in CCI-TBI mechanisms.

EXPERIMENTAL METHODS

Animals and Reagents. Adult mice of 4−5 months of age, strain C57BL/6J, females, were obtained from Jackson Laboratories (Bar Harbor, Maine). Mice were housed in the vivarium at UC San Diego for at least 1 week prior to experiments. Mice were housed at 3−5 mice per cage, under standard conditions with ad libitum access to food and water. Care of mice was conducted in compliance with protocols approved by the Institutional Animal Care and Use Committee at the University of California, San Diego, and in accordance with the NIH Guide for the Care and Use of Laboratory Animals.

Reagents for mouse anesthesia consisted of isoflurane from VetOne (Boise, ID), buprenorphine from Par Pharmaceuticals (Chestnut Ridge, NY), and ketamine from Zoetis (Parsippany, NJ). The substrate reagent Z-Nle-Lys-Arg-AMC for cathepsin B was from the Genscript company (Piscataway, NJ). Recombinant mouse cathepsin B was from R & D Systems (Minneapolis, MN) and the substrate Z-Phe-Arg-AMC was from Genscript. Mouse cathepsins C, H, L, and X were from R & D Systems (Minneapolis, MN); substrates GR-AMC, R-AMC, Z-FR-AMC were from Genscript (Piscataway, NJ), and MCA-Arg-Pro-Pro-Gly-Phe-Ser-Ala-Phe-Lys(Dnp)OH substrate was from R & D Systems (MN). For cathepsin B localization in mouse brain, an antibody (goat) to mouse cathepsin B was from R & D Systems (Minneapolis, MN). Prolong gold with DAPI and donkey antigoat IgG, A-488 conjugated were from Thermo Fisher Scientific (Waltham, MA). Cresyl violet and Entellan mounting medium were from Sigma (Burlington, MA). The protein assay kit was from Biorad (Hercules, CA).

Controlled Cortical Impact (CCI) Mouse Model of TBI (CCI-TBI). Mice were anesthetized with 3% isoflurane (VetOne, Boise, ID) and a 1.0 L per minute flow rate of oxygen and secured in a stereotaxic frame (Kopf, Tujunga, CA) with isoflurane anesthesia. During anesthesia, mice were on a 37 °C warming pad (RWD Life Science, San Diego, CA). The fur was shaved from the top of the head, and the scalp was sterilized with Betadine and 70% ethanol. An incision was made from the orbital area to the posterior edge of the skull and retracted with an alm retractor (Kent Scientific, Torrington, CT). For mice receiving CCI-TBI to the right motor cortex, a 5 mm craniotomy was made spanning from 0.5 to 5.5 mm posterior of bregma, and 1 to 6 mm right of the sagittal suture with a stereotaxic microdrill (RWD Life Science). The impact was performed at the craniotomy site using a MyNeuroLab Impact One Stereotaxic Impactor (Leica, Teaneck, NJ), with a 3 mm impactor tip, impact speed of 3 m/s, to a depth of 1 mm, and a 100 ms dwell time. A 5 mm circular sterile glass coverslip (Electron Microscopy Sciences, Hatfield, PA) was placed on the impact site, and the incision was closed with GLUture (Abbot Laboratories, Chicago, IL). Mice received 5 mg/kg of buprenorphine analgesic (Par Pharmaceuticals, Irvine, CA) immediately after CCI-TBI. Mice were monitored for several hours after CCI-TBI and received an additional 5 mg/kg of buprenorphine before returning to the vivarium. Control sham mice received anesthesia and an incision in the skin at the top of the head.

Rotarod Performance Assay for Motor Function. Motor function was assessed by the rotarod assay for naïve adult mice, mice subjected to sham control, and mice subjected to CCI-TBI. At 2 days before the sham or CCI procedure, five training trials were conducted composed of trial 1 consisting of 5−10 rpm during 120 s, trial 2 consisting of 5−20 rpm during 240 s, and trials 3 to 5 each consisting of 5−40 rpm during 240 s. Rotarod baseline assay trials were conducted 1 day before the sham or CCI procedures. Rotarod performance was assessed after the CCI-TBI and sham procedures on designated days during a 1 week period. Each day of rotarod testing consisted of triplicate trials consisting of 5−40 rpm over 240 s. The latency time that mice remained on the rotating beam before falling was determined. If a mouse remained on the rotating beam for 240 s, the latency time was recorded as 240 s. Data are expressed as mean latency (secs) ± sem or % baseline latency ± sem for each day of testing. Significance was determined by student's t-test of $p < 0.05$ comparing CCI-TBI to the control sham.

Brain Cortex and Hippocampus Collection. For the collection of brain cortex and hippocampus, mice were sacrificed by anesthesia with 200 mg/kg ketamine. Blood was collected by liver vein portal, and mice were then perfused with 14 mL of sterile normal saline for collection of brain tissue for biochemical cathepsin B analyses or with 14 mL of sterile normal saline followed by 21 mL of 4% paraformaldehyde for Nissl histology and immunofluorescence microscopy.

Preparation of Homogenate and Cytosol Fraction Samples from Brain Tissues. Fresh brain cortex and hippocampus tissue homogenates, from ipsilateral and contralateral hemispheres, were subjected to homogenization in 5 mL of 0.32 M ice-cold sucrose with a 15 mL glass-Teflon Potter-Elvehjen Tissue Grinder with 0.11−0.15 cm clearance (Thomas Scientific, Swedesboro, NJ) at 900 rpm for 12 strokes of 5 s each with an overhead stirrer (Wheaton, Millville, NJ) with samples on ice. An aliquot of the homogenate was retained for the cathepsin B assays.

For cortex samples, cytosol was isolated from the homogenate by centrifugation at 1000g for 5 min to pellet nuclei and cell debris (P1). The supernatant (S1) was centrifuged at 12,000g for 20 min to pellet lysosomes, synaptosomes, and mitochondria (P2 fraction). The cytosol-containing fraction (S2) was collected for the cathepsin B activity assays. This method for cytosol preparation and subcellular fractionation was conducted as described by Gray and Whittaker[36] and by Wegrzyn et al.[37]

The protein concentrations in brain homogenates and isolated cytosol samples were measured by the Biorad colorimetric protein assay kit (Biorad reagents A and B, catalogue numbers 5000113 and 5000114).

Cathepsin B Activity Assay of Brain Samples. Cathepsin B activity in homogenate, cytosol, and P2 lysosomal brain samples was monitored with the substrate Z-Nle-Lys-Arg-AMC. This substrate specifically detects cathepsin B activity and not other cysteine cathepsins.[23] Cathepsin B activity assays of tissue samples were conducted in 40 mM citrate-phosphate buffer (pH 5.5 or pH 7.2), 5.0

https://doi.org/10.1021/acschemneuro.4c00577
ACS Chem. Neurosci. 2025, 16, 1297−1308

mM DTT, 1.0 mM EDTA, 100 mM NaCl, and 60 μM Z-Nle-Lys-Arg-AMC with incubation at 37 °C for 30 min, followed by quantitation of AMC fluorescence at 460 nm excitation and 360 nm emission measured on a Synergy HTX plate reader (BioTek, Winooski, VT), as described by our group.[23]

Samples for cathepsin B assays consisted of cortex homogenate of 2−3 μg protein/assay (8 μL of 1:5 dilution per assay), hippocampus homogenate of 2−5 μg protein/assay (5 ul of 1:5 dilution per assay), and cytosol fraction (from cortex) of 8−14 μg protein/assay (20 μL/assay). Assays for each sample were conducted in triplicate. Fluorescence was converted to pmol AMC using a standard plot of AMC standards at 0, 10, 20, 50, and 100 μM. Data for cathepsin B activity are reported as the mean of pmol AMC per μg protein for a 30 min assay, with standard error of the mean (sem). Significance was determined by student's *t*-test with $p < 0.05$.

For comparison of cathepsin B activity in ipsilateral and contralateral brain cortex or hippocampus regions, significance was assessed by both paired and unpaired *t*-tests with $p < 0.05$. Paired and unpaired *t*-tests both indicated significance or no significance for the same paired comparisons of ipsilateral compared to contralateral cathepsin B activity. Note that our studies were focused on comparing two groups per experiment for ipsilateral and contralateral data and, therefore, we did not conduct post hoc correction for multiple comparisons.[38]

Brain Histology and Lesion Volume Analyses. Nissl staining (using cresyl violet) of brain sections provided histological assessment of normal and sham brain cortex and hippocampus tissue integrity and lesions. Tissue sections were mounted on superfrost positively charged slides (Fisher Scientific, Waltham, MA) and were dried overnight at 37 °C, fixed in 10% formalin, rinsed, and incubated with Nissl stain (Nissl stain consisting of 0.25% cresyl violet acetate in water) for 5 min. Slides were rehydrated sequentially with ethanol at 100, 95, 70, and 50% for 1 min each. Sections were then cleared of dehydrating reagents with Citrisolv (Decon Laboratories) for 10 min. Nissl-stained sections were scanned at 20× magnification with a NanoZoomer S60 Digital Slide Scanner (Hamamatsu). Regions of interest were assessed using NDP.View2 and were analyzed with ImageJ. Areas of cortical tissue loss were quantitated and compared to the whole hemisphere to assess % cortical tissue loss.

Qualitative analysis of the cortical and hippocampus regions following CCI-TBI was performed for Nissl-stained sections at −1.75 bregma using a scale rating of 0−5, comparing the ipsilateral hemisphere containing CCI-TBI to the contralateral hemisphere. These histological analyses assessed 8 brain sections per animal for each of the cortex and hippocampus regions, and two CCI-TBI animals and two sham control animals were assessed. All brain sections were subjected to identical procedures (described in this Method section) that maintained consistency for all samples.

The histology of the hippocampus was assessed for integrity or disorganization by a rating scale consisting of "0" for normal hippocampus structure, "1" for minor architectural alterations, "2" for major architectural alterations, "3" for major architectural alterations with loss of cells, and '4' for complete loss of hippocampus (shown in supplemental Figure S2).

Cathepsin B Immunofluorescence Microscopy. Brain sections were rinsed with PBS and blocked with 10% normal donkey serum (NDS) with 0.3% Triton X-100 for 1 h. After PBS rinsing, sections were incubated with goat anti-mouse cathepsin B (R&D Systems) for 24 h. Following washing with PBS, sections were incubated with donkey antigoat IgG conjugated with AlexaFluor 488 for 1 h (Thermo Fisher Scientific). Sections were washed with PBS, received Prolong Gold with DAPI (Thermo Fisher Scientific), and covered.

Cathepsin B immunostaining was imaged with a Leica DMI8000 confocal microscope with a 63X objective. Immunostaining was evaluated at −1.75 bregma at the cortex and hippocampus regions on the ipsilateral side of CCI-TBI, and similar locations were imaged on the contralateral side of the brain. These immunofluorescence assays assessed two brain sections for each CCI-TBI animal, consisting of one for the cortex and another for the hippocampus. Each brain section image displayed approximately 100 cells, and thus, about 200 cells were analyzed from two brain sections for each condition of CCI-TBI and sham. Immunofluorescence was conducted for two CCI-TBI mice and two sham mice. Cathepsin B punctate localization was determined with ImageJ by using the Coloc2 plugin. The normal punctate lysosomal of cathepsin B was located adjacent to the nuclei (stained by DAPI); thus, quantitation of punctate cathepsin B immunofluorescence was related to percent colocalization with nuclei (stained by DAPI) determined with ImageJ assessed using the Coloc2 plugin and Pearson's coefficient analysis.[39,40]

Synthesis of Z-Arg-Lys-AOMK Inhibitor. Z-Arg-Lys-AOMK was synthesized as we have reported.[41] Briefly, Fmoc-Lys(boc)-$COCH_2Cl$ was acylated with 2,6-dimethylbonzoic acid to produce Fmoc-Lys-(boc)-AOMK. Fmoc was removed by Pd-catalyzed hydrogenation using mildly acidic conditions. The resulting deprotected ammonium chloride salt was coupled with Z-Arg-$(boc)_2$-OH, and Z-Arg-Lys-AOMK was obtained as the TFA salt by TFA deprotection of the three Boc groups. The resulting Z-Arg-Lys-AOMK was analyzed by LC-MS[42,43] to confirm the molecular weight identity of the inhibitor $[M + H]^+$ peak (supplemental Figure S5), which confirmed the structure of the product and its purity of more than 95%.

Inhibition of Recombinant Mouse Cathepsin B by Z-Arg-Lys-AOMK. Recombinant mouse cathepsin B (R&D Systems) was activated in 20 mM sodium acetate, pH 5.5, 100 mM NaCl (Fisher Chemicals, Pittsburgh, PA), 1 mM EDTA (Calbiochem, Burlington, MA), 5 mM dithiothreitol (DTT, Promega, Madison, WI) for 30 min at 37 °C. After activation, 0.04 ng/μL cathepsin B activity was assayed in 40 mM citrate-phosphate buffer adjusted to pH 4.6 or pH 7.2, with 100 mM NaCl, 1 mM EDTA, 5 mM DTT, 0.01% Tween-20 and 1.5% DMSO at room temperature. Cathepsin B activity was measured with 40 μM Z-Phe-Arg-AMC and with Z-Arg-Lys-AOMK inhibitor concentrations serially diluted 1.5-fold from 5536 to 1.7 nM. Each condition was conducted in quadruplicates in black 384 well plates. Substrate and inhibitor solutions were initially combined, then the enzyme was added, and the readings were recorded with a BioTek plate reader immediately afterward. Activity was recorded as relative fluorescence units per second (RFU/s). RFU parameters were: excitation at 360 nm, emission at 460 nm, gain of 50, and top optics with read height at 1 mm from the assay plate. Activity values were recorded as the highest slope detected in 10 consecutive readings, 46 s each, for 30 min. Data are expressed as % relative activity of cathepsin B, in the presence of inhibitor relative to the 'no inhibitor' DMSO control condition. The potency of inhibitor reduction of cathepsin B activity was assessed by IC_{50} values, the concentration of inhibitor that reduced cathepsin B activity by 50%.

Evaluation of the Specificity of Z-Arg-Lys-AOMK for the Inhibition of Purified Mouse Cathepsin B Compared to Mouse Cathepsins C, H, L, and X. Mouse cathepsins C, H, L, and X (recombinant) were assayed with substrates Gly-Arg-AMC, Arg-AMC, Z-Phe-Arg-AMC, and MCA-Arg-Pro-Pro-Gly-Phe-Ser-Ala-Phe-Lys(Dnp)OH, respectively. Mouse cathepsins C, H, L, and X were activated according to the manufacturer's instructions (R&D, Minneapolis MN). Cathepsin protease assays were conducted in the absence and presence of Z-Arg-Lys-AOMK at different concentrations from 10 nM to 10 μM. Assay conditions for these mouse cathepsins C, H, O, and X consisted of 40 mM citrate phosphate buffer at pH 7.2 or pH 4.6, 5 mM DTT, 1 mM EDTA, 100 mM NaCl, and 40 μM substrate, with incubation at room temperature for 30 min. Fluorescence was read by a BioTek plate reader for excitation at 360 nm and emission at 460 nm for all substrates, except for assays using MCA-Arg-Pro-Pro-Gly-Phe-Ser-Ala-Phe-Lys(Dnp)OH which used excitation of 320 nm and emission at 400 nm for fluorescence readings.

Administration of Z-Arg-Lys-AOMK to CCI-TBI Mice and Evaluation of Cathepsin B Activity with Rotarod Assessment. Mice were injected intraperitoneally (ip) with 20 mg/kg Z-Arg-Lys-AOMK in 17% DMSO in 0.9% NaCl, or with vehicle control consisting of 17% DMSO in 0.9% NaCl. Inhibitor administration consisted of i.p. injection of 250 μL of 2 mg/mL Z-Arg-Lys-AOMK in 17% DMSO and sterile 0.9% NaCl. For vehicle control, injections consisted of 17% DMSO in sterile 0.9% NaCl.

https://doi.org/10.1021/acschemneuro.4c00577
ACS Chem. Neurosci. 2025, 16, 1297−1308

Statistical Analyses. Data for rotarod assay and cathepsin B activity were compared for CCI-TBI and sham conditions by student's *t*-test and significance determined with $p < 0.05$, with the calculation of the mean and stand error of the mean (sem).

Cortical lesion volumes in CCI-TBI compared to sham were determined quantitatively by measuring lesion volume in the side of the brain ipsilateral to CCI-TBI compared to the contralateral, uninjured, side of the brain for each mouse using ImageJ software. The significance of % cortical tissue loss between CCI-TBI and sham was compared by student's *t*-test with $p < 0.05$, for the mean with sem.

Hippocampal disorganization was evaluated by the scoring of "0" for normal hippocampus structure, "1" for minor architectural alterations, "2" for major architectural alterations, "3" for major architectural alterations accompanied by loss of cells, and "4" for complete loss of hippocampus. Scores were averaged and significance was determined with student's *t*-test with a significance of $p < 0.05$.

For cathepsin B immunofluorescence intensity and cellular distribution, green immunofluorescent puncta features were assessed for area and intensity with the Coloc2 plugin of ImageJ software. Quantitative values indicated the % of cathepsin B immunofluorescence in puncta features in CCI-TBI compared to the sham. Graphs indicate mean % puncta fluorescence with error bars indicating sem. Graphs of data were prepared with Prism v 10.2.2 (GraphPad).

■ ASSOCIATED CONTENT

Supporting Information

The Supporting Information is available free of charge at https://pubs.acs.org/doi/10.1021/acschemneuro.4c00577.

> Sham mice with craniotomy and motor function; hippocampus disorganization; cathepsin B activity in cytosol and lysosomal fraction; inhibitor mass spectrometry; mouse cathepsins; and Z-R-K-AOMK inhibitor (PDF)

■ AUTHOR INFORMATION

Corresponding Author

Vivian Hook − *Skaggs School of Pharmacy and Pharmaceutical Sciences and Department of Neurosciences and Department of Pharmacology, School of Medicine, University of California, San Diego, La Jolla, California 92093, United States;* orcid.org/0000-0001-6461-7024; Email: vhook@ucsd.edu

Authors

Sonia Podvin − *Skaggs School of Pharmacy and Pharmaceutical Sciences, University of California, San Diego, La Jolla, California 92093, United States*

Jazmin Florio − *Department of Physiology and Neuroscience, USC Alzheimer's Therapeutic Research Institute, San Diego, California 92121, United States*

Brian Spencer − *Department of Physiology and Neuroscience, USC Alzheimer's Therapeutic Research Institute, San Diego, California 92121, United States*

Michael Mante − *Department of Physiology and Neuroscience, USC Alzheimer's Therapeutic Research Institute, San Diego, California 92121, United States*

Estefani Guzman − *Department of Physiology and Neuroscience, USC Alzheimer's Therapeutic Research Institute, San Diego, California 92121, United States*

Carlos Arias − *Department of Physiology and Neuroscience, USC Alzheimer's Therapeutic Research Institute, San Diego, California 92121, United States*

Charles Mosier − *Skaggs School of Pharmacy and Pharmaceutical Sciences, University of California, San Diego, La Jolla, California 92093, United States*

Von V. Phan − *Skaggs School of Pharmacy and Pharmaceutical Sciences and Biomedical Sciences Graduate Program, University of California, San Diego, La Jolla, California 92093, United States*

Michael C. Yoon − *Skaggs School of Pharmacy and Pharmaceutical Sciences, University of California, San Diego, La Jolla, California 92093, United States;* orcid.org/0000-0002-2900-5257

Jehad Almaliti − *Center for Marine Biotechnology and Biomedicine, Scripps Institution of Oceanography, University of California, San Diego, La Jolla, California 92093, United States; Department Pharmaceutical Sciences, College of Pharmacy, The University of Jordan, Amman 11942, Jordan*

Anthony J. O'Donoghue − *Skaggs School of Pharmacy and Pharmaceutical Sciences, University of California, San Diego, La Jolla, California 92093, United States*

William H. Gerwick − *Center for Marine Biotechnology and Biomedicine, Scripps Institution of Oceanography, University of California, San Diego, La Jolla, California 92093, United States;* orcid.org/0000-0003-1403-4458

Robert A. Rissman − *Department of Physiology and Neuroscience, USC Alzheimer's Therapeutic Research Institute, San Diego, California 92121, United States*

Complete contact information is available at: https://pubs.acs.org/10.1021/acschemneuro.4c00577

Author Contributions

Research design of animal experiments was conducted by V.H., R.A.R., S.P., J.F., and M.M.; Animal rotarod assays for evaluation of motor function were conducted by E.G., M.M., and J.F.; Inhibitor (Z-Arg-Lys-AOMK) chemical synthesis design and planning were conducted by J.A., W.H.G., and A.J.O.; Biochemical characterization of cathepsin B was conducted by C.M., V.V.P., and M.C.Y.; Data analysis was conducted by all authors, led by V.H., R.A.R., S.P., and J.F.; Manuscript writing was conducted by S.P. and V.H., with review and editing by all authors.

Notes

The authors declare the following competing financial interest(s): V. Hook has an equity position at American Life Science Pharmaceuticals (ALSP) and is a founder of ALSP. V. Hook is an advisor to ALSP. V. Hook's conflict has been disclosed and is managed by her employer, the University of California, San Diego. The other authors have no conflicts of interest.

■ ACKNOWLEDGMENTS

This research was supported by NIH grant R01NS109075 awarded to VH and grant R01AG079303 awarded to RR. V.V.P. was supported by T32 AG066596 (awarded to E. Koo and J. Brewer) and by T32 GM153123 (awarded to J. Heller Brown and T. Handel). MCY was supported by NIH T32GM067550 (awarded to W.H.G.). The UC San Diego Microscopy Imaging Core was supported by NIH P30NS047101 (awarded to B. Zheng). J.A. acknowledges the St. Baldrick's Foundation for the International Scholar Award 2022-2025 (Award #940892) and the Deanship of Scientific Research at the University of Jordan for his scientific sabbatical leave.

REFERENCES

(1) Hook, G.; Reinheckel, T.; Ni, J.; Wu, Z.; Kindy, M.; Peters, C.; Hook, V. Cathepsin B Gene Knockout Improves Behavioral Deficits and Reduces Pathology in Models of Neurologic Disorders. *Pharmacol Rev.* **2022**, *74* (3), 600−629.

(2) Assfalg-Machleidt, I.; Jochum, M.; Nast-Kolb, D.; Siebeck, M.; Billing, A.; Joka, T.; Rothe, G.; Valet, G.; Zauner, R.; Scheuber, H. P.; et al. Cathepsin B-indicator for the release of lysosomal cysteine proteinases in severe trauma and inflammation. *Biol. Chem. Hoppe Seyler* **1990**, *371* (Suppl), 211−222.

(3) Jochum, M; Machleidt, W; Friz, H. *Phagocyte proteinases in multiple trauma and sepsi: pathomechanisms and related therapeutic approaches in Handbook of Mediators in Septic Shock*; Neugebauer, E. A.; Holaday, J. W., Eds.; CRC Press: Boca Raton, FL: 1993; pp 336−361.

(4) Sundelöf, J.; Sundström, J.; Hansson, O.; Eriksdotter-Jönhagen, M.; Giedraitis, V.; Larsson, A.; Degerman-Gunnarsson, M.; Ingelsson, M.; Minthon, L.; Blennow, K.; Kilander, L.; Basun, H.; Lannfelt, L. Higher cathepsin B levels in plasma in Alzheimer's disease compared to healthy controls. *J. Alzheimers Dis.* **2011**, *22* (4), 1223−1230.

(5) Sun, Y.; Rong, X.; Lu, W.; Peng, Y.; Li, J.; Xu, S.; Wang, L.; Wang, X. Translational study of Alzheimer's disease (AD) biomarkers from brain tissues in AβPP/PS1 mice and serum of AD patients. *J. Alzheimers Dis.* **2015**, *45* (1), 269−282.

(6) Hook, G. R.; Yu, J.; Sipes, N.; Pierschbacher, M. D.; Hook, V.; Kindy, M. S. The cysteine protease cathepsin B is a key drug target and cysteine protease inhibitors are potential therapeutics for traumatic brain injury. *J. Neurotrauma.* **2014**, *31* (5), 515−529.

(7) Kindy, M. S.; Yu, J.; Zhu, H.; El-Amouri, S. S.; Hook, V.; Hook, G. R. Deletion of the cathepsin B gene improves memory deficits in a transgenic ALZHeimer's disease mouse model expressing AβPP containing the wild-type β-secretase site sequence. *J. Alzheimers Dis.* **2012**, *29* (4), 827−840.

(8) Hook, G.; Yu, J.; Toneff, T.; Kindy, M.; Hook, V. Brain pyroglutamate amyloid-β is produced by cathepsin B and is reduced by the cysteine protease inhibitor E64d, representing a potential Alzheimer's disease therapeutic. *J. Alzheimers Dis.* **2014**, *41* (1), 129−149.

(9) Wu, Z.; Ni, J.; Liu, Y.; Teeling, J. L.; Takayama, F.; Collcutt, A.; Ibbett, P.; Nakanishi, H. Cathepsin B plays a critical role in inducing Alzheimer's disease-like phenotypes following chronic systemic exposure to lipopolysaccharide from Porphyromonas gingivalis in mice. *Brain Behav Immun.* **2017**, *65*, 350−361.

(10) Mielke, M. M.; Ransom, J. E.; Mandrekar, J.; Turcano, P.; Savica, R.; Brown, A. W. Traumatic Brain Injury and Risk of Alzheimer's Disease and Related Dementias in the Population. *J. Alzheimers Dis.* **2022**, *88* (3), 1049−1059.

(11) Dams-O'Connor, K.; Guetta, G.; Hahn-Ketter, A. E.; Fedor, A. Traumatic brain injury as a risk factor for Alzheimer's disease: current knowledge and future directions. *Neurodegener Dis Manag.* **2016**, *6* (5), 417−429.

(12) Li, Y.; Li, Y.; Li, X.; Zhang, S.; Zhao, J.; Zhu, X.; Tian, G. Head Injury as a Risk Factor for Dementia and Alzheimer's Disease: A Systematic Review and Meta-Analysis of 32 Observational Studies. *PLoS One.* **2017**, *12* (1), No. e0169650.

(13) Repnik, U.; Turk, B. Lysosomal-mitochondrial cross-talk during cell death. *Mitochondrion.* **2010**, *10* (6), 662−669.

(14) de Castro, M. A.; Bunt, G.; Wouters, F. S. Cathepsin B launches an apoptotic exit effort upon cell death-associated disruption of lysosomes. *Cell Death Discovery* **2016**, *29* (2), 16012.

(15) Hentze, H.; Lin, X. Y.; Choi, M. S.; Porter, A. G. Critical role for cathepsin B in mediating caspase-1-dependent interleukin-18 maturation and caspase-1-independent necrosis triggered by the microbial toxin nigericin. *Cell Death Differ.* **2003**, *10* (9), 956−968.

(16) Bai, H.; Yang, B.; Yu, W.; Xiao, Y.; Yu, D.; Zhang, Q. Cathepsin B links oxidative stress to the activation of NLRP3 inflammasome. *Exp. Cell Res.* **2018**, *362* (1), 180−187.

(17) Campden, R. I.; Zhang, Y. The role of lysosomal cysteine cathepsins in NLRP3 inflammasome activation. *Arch. Biochem. Biophys.* **2019** Jul 30;*670*:32−42.

(18) Hernandez, M. L.; Marone, M.; Gorse, K. M.; Lafrenaye, A. D. Cathepsin B Relocalization in Late Membrane Disrupted Neurons Following Diffuse Brain Injury in Rats. *ASN Neuro.* **2022**, *14*, No. 17590914221099112.

(19) Belinson, H.; Lev, D.; Masliah, E.; Michaelson, D. M. Activation of the amyloid cascade in apolipoprotein E4 transgenic mice induces lysosomal activation and neurodegeneration resulting in marked cognitive deficits. *J. Neurosci.* **2008**, *28* (18), 4690−4701.

(20) Yang, A. J.; Chandswangbhuvana, D.; Margol, L.; Glabe, C. G. Loss of endosomal/lysosomal membrane impermeability is an early event in amyloid Abeta1−42 pathogenesis. *J. Neurosci Res.* **1998**, *52* (6), 691−698.

(21) Ditaranto, K.; Tekirian, T. L.; Yang, A. J. Lysosomal membrane damage in soluble Abeta-mediated cell death in Alzheimer's disease. *Neurobiol Dis.* **2001**, *8* (1), 19−31.

(22) Luo, C. L.; Chen, X. P.; Li, L. L.; Li, Q. Q.; Li, B. X.; Xue, A. M.; Xu, H. F.; Dai, D. K.; Shen, Y. W.; Tao, L. Y.; Zhao, Z. Q. Poloxamer 188 attenuates in vitro traumatic brain injury-induced mitochondrial and lysosomal membrane permeabilization damage in cultured primary neurons. *J. Neurotrauma.* **2013**, *30* (7), 597−607.

(23) Yoon, M. C.; Solania, A.; Jiang, Z.; Christy, M. P.; Podvin, S.; Mosier, C.; Lietz, C. B.; Ito, G.; Gerwick, W. H.; Wolan, D. W.; Hook, G.; O'Donoghue, A. J.; Hook, V. Selective Neutral pH Inhibitor of Cathepsin B Designed Based on Cleavage Preferences at Cytosolic and Lysosomal pH Conditions. *ACS Chem. Biol.* **2021** Sep 17;*16*(9):1628−1643.

(24) Valera, E. M.; Joseph, A. C.; Snedaker, K.; Breiding, M. J.; Robertson, C. L.; Colantonio, A.; Levin, H.; Pugh, M. J.; Yurgelun-Todd, D.; Mannix, R.; Bazarian, J. J.; Turtzo, L. C.; Turkstra, L. S.; Begg, L.; Cummings, D. M.; Bellgowan, P. S. F. Understanding Traumatic Brain Injury in Females: A State-of-the-Art Summary and Future Directions. *J. Head Trauma Rehabil.* **2021**, *36* (1), E1−E17.

(25) Cogan, A. M.; McCaughey, V. K.; Scholten, J. Gender Differences in Outcomes after Traumatic Brain Injury among Service Members and Veterans. *PM R.* **2020**, *12* (3), 301−314.

(26) Breeding, T.; Martinez, B.; Katz, J.; Nasef, H.; Santos, R. G.; Zito, T.; Elkbuli, A. The Association Between Gender and Clinical Outcomes in Patients With Moderate to Severe Traumatic Brain Injury: A Systematic Review and Meta-Analysis. *J. Surg Res.* **2024**, *295*, 791−799.

(27) Mikolić, A.; van Klaveren, D.; Groeniger, J. O.; Wiegers, E. J. A.; Lingsma, H. F.; Zeldovich, M.; von Steinbüchel, N.; Maas, A. I. R.; Roeters van Lennep, J. E.; Polinder, S. CENTER-TBI Participants and Investigators. Differences between Men and Women in Treatment and Outcome after Traumatic Brain Injury. *J. Neurotrauma* **2021**, *38* (2), 235−251.

(28) Starkey, N. J.; Duffy, B.; Jones, K.; Theadom, A.; Barker-Collo, S.; Feigin, V.; BIONIC8 Research Group. Sex differences in outcomes from mild traumatic brain injury eight years post-injury. *PLoS One* **2022**, *17* (5), No. e0269101.

(29) Yoon, M. C.; Phan, V.; Podvin, S.; Mosier, C.; O'Donoghue, A. J.; Hook, V. Distinct Cleavage Properties of Cathepsin B Compared to Cysteine Cathepsins Enable the Design and Validation of a Specific Substrate for Cathepsin B over a Broad pH Range. *Biochemistry.* **2023**, *62* (15), 2289−2300.

(30) Hernandez, M.; Regan, S.; Ansari, R.; Logan-Wesley, A.; Lilova, R.; Levi, C.; Gorse, K.; Lafrenaye, A. The Effects of Cathepsin B Inhibition in the Face of Diffuse Traumatic Brain Injury and Secondary Intracranial Pressure Elevation. *Biomedicines.* **2024**, *12* (7), 1612.

(31) Lafrenaye, A. D.; McGinn, M. J.; Povlishock, J. T. Increased intracranial pressure after diffuse traumatic brain injury exacerbates neuronal somatic membrane poration but not axonal injury: evidence for primary intracranial pressure-induced neuronal perturbation. *J. Cereb Blood Flow Metab.* **2012**, *32* (10), 1919−1932.

https://doi.org/10.1021/acschemneuro.4c00577
ACS Chem. Neurosci. 2025, 16, 1297−1308

(32) Boutté, A. M.; Hook, V.; Thangavelu, B.; Sarkis, G. A.; Abbatiello, B. N.; Hook, G.; Jacobsen, J. S.; Robertson, C. S.; Gilsdorf, J.; Yang, Z.; Wang, K. K. W.; Shear, D. A. Penetrating Traumatic Brain Injury Triggers Dysregulation of Cathepsin B Protein Levels Independent of Cysteine Protease Activity in Brain and Cerebral Spinal Fluid. *J. Neurotrauma.* **2020**, *37* (13), 1574−1586.
(33) Yu, J.; Zhu, H.; Taheri, S.; Monday, W. L.; Perry, S.; Kindy, M. S. Reduced Neuroinflammation and Improved Functional Recovery after Traumatic Brain Injury by Prophylactic Diet Supplementation in Mice. *Nutrients.* **2019**, *11* (2), 299.
(34) Nakanishi, H. Microglial cathepsin B as a key driver of inflammatory brain diseases and brain aging. *Neural Regen Res.* **2020**, *15* (1), 25−29.
(35) Terada, K.; Yamada, J.; Hayashi, Y.; Wu, Z.; Uchiyama, Y.; Peters, C.; Nakanishi, H. Involvement of cathepsin B in the processing and secretion of interleukin-1beta in chromogranin A-stimulated microglia. *Glia.* **2010**, *58* (1), 114−124.
(36) Gray, E.; Whittaker, V. The isolation of nerve endings from brain: an electron microscopic study of cell fragments derived by homogenization and centrifugation. *J. Anat.* **1962**, *96*, 79−88.
(37) Wegrzyn, J. L.; Bark, S. J.; Funkelstein, L.; Mosier, C.; Yap, A.; Kazemi-Esfarjani, P.; La Spada, A. R.; Sigurdson, C.; O'Connor, D. T.; Hook, V. Proteomics of dense core secretory vesicles reveal distinct protein categories for secretion of neuroeffectors for cell-cell communication. *J. Proteome Res.* **2010**, *9* (10), 5002−5024.
(38) Lee, S.; Lee, D. K. What is the proper way to apply the multiple comparison test? *Korean J. Anesthesiol.* **2018**, *71* (5), 353−360.
(39) Stauffer, W.; Sheng, H.; Lim, H. N. EzColocalization: An ImageJ plugin for visualizing and measuring colocalization in cells and organisms. *Sci. Rep.* **2018**, *8* (1), 15764.
(40) Moser, B.; Hochreiter, B.; Herbst, R.; Schmid, J. A. Fluorescence colocalization microscopy analysis can be improved by combining object-recognition with pixel-intensity-correlation. *Biotechnol. J.* **2017**, *12* (1), No. 1600332.
(41) Almaliti, J.; Alhindy, M.; Yoon, M. C.; Hook, V.; Molinski, T. F.; O'Donoghue, A. J.; Gerwick, W. H. Orthogonal Deprotection Strategy of Fmoc Provides Improved Synthesis of Sensitive Peptides: Application to Z-Arg-Lys-AOMK. *ACS Omega* **2024**, *9* (3), 3997−4003.
(42) Winnikoff, J. R.; Glukhov, E.; Watrous, J.; Dorrestein, P. C.; Gerwick, W. H. Quantitative molecular networking to profile marine cyanobacterial metabolomes. *J. Antibiot (Tokyo).* **2014**, *67* (1), 105−112.
(43) O'Rourke, A.; Kremb, S.; Duggan, B. M.; Sioud, S.; Kharbatia, N.; Raji, M.; Emwas, A. H.; Gerwick, W. H.; Voolstra, C. R. Identification of a 3-Alkylpyridinium Compound from the Red Sea Sponge *Amphimedon chloros* with *In Vitro* Inhibitory Activity against the West Nile Virus NS3 Protease. *Molecules.* **2018**, *23* (6), 1472.
(44) Bright, G. R.; Fisher, G. W.; Rogowska, J.; Taylor, D. L. Fluorescence ratio imaging microscopy: temporal and spatial measurements of cytoplasmic pH. *J. Cell Biol.* **1987**, *104*, 1019−1033.
(45) Mindell, J. A. Lysosomal acidification mechanisms. *Annu. Rev. Physiol.* **2012**, *74*, 69−86.

https://doi.org/10.1021/acschemneuro.4c00577
ACS Chem. Neurosci. 2025, 16, 1297−1308